Chem Rev Lett 9 (2026) 230-242

Research Article

Chemical Review and Letters
journal homepage: www.chemrevlett.com
ISSN (online): 2645-4947 (print) 2676-7279

DFT studies on HCN gas detection by pristine and Li decorated Triazasumanene nanostructures

Odil Narkulov[1,*], Ugiloy Nuraliyevna Soxibova[2], Ulugbek Qalandarov[3], Xurshida Urunova[4], Gulrukh Haydarova[5], Lola Shukurovna Boliyeva[6], Gulruh Matchanova[7], Nargizakhon Qodirova[8], Utkir Pardaboyev[9], Sadridin Eshkaraev[10]

[1]*Department of Pedagogy, University of Economics and Pedagogy, Karshi, Uzbekistan.*
[2]*Department of Applied English, Tashkent State Technical University named after Islam Karimov, Tashkent, Uzbekistan.*
[3]*Department of Economics and Engineering, University of Economics and Pedagogy, Uzbekistan.*
[4]*Department of Agronomy, Navoi State University of Mining and Technology, Navoi, Uzbekistan.*
[5]*Department of Theory and Practice of Preschool and Primary Education, Faculty of Preschool and Primary Education, Chirchik State Pedagogical University, Chirchik, Uzbekistan.*
[6]*Department of Pedagogy Preschool Education, Chirchik State Pedagogical University, 111700, Chirchik, Uzbekistan.*
[7]*Department of Technologies and Equipment of Light Industry, Urgench State University named after Abu Raykhan Beruni, Urgench, Uzbekistan.*
[8]*Andijan State Institute for Foreign Languages, Andijan, Uzbekistan.*
[9]*Department of Vehicle Engineering, Jizzakh Polytechnic Institute, Jizzakh, Uzbekistan.*
[10]*Department of Medicine, Termez University of Economics and Service, Termez, Uzbekistan.*

ARTICLE INFO

Article history:
Received 26 November 2025
Received in revised form 27 December 2025
Accepted 01 January 2026

Keywords:
HCN
DFT
Adsorption
Triazasumanene
Detection

ABSTRACT

This research employed density functional theory (DFT) calculations to assess the potential of both unmodified and lithium-enhanced Triazasumanene (TAS) nanostructures as sensors for detecting the hazardous hydrogen cyanide (HCN) gas. The findings from adsorption energy and thermodynamic parameter analysis indicated that pristine TAS interacts weakly with HCN, showing minimal changes in its bandgap (Eg). To improve its sensing capability, TAS was altered by incorporating a lithium atom, resulting in Li@TAS. The calculated negative adsorption energies and thermodynamic data suggested that HCN adsorption on Li@TAS is thermodynamically favorable, exothermic, and spontaneous under experimental conditions. The density of states analysis revealed a notable 8.38% reduction in the bandgap of Li@TAS, decreasing from 1.49 eV to 1.36 eV. Further exploration of interaction characteristics through NCI and RDG analyses demonstrated a strong bond between the nitrogen atom of HCN and the lithium atom on the modified TAS. Additionally, NBO charge analysis confirmed significant charge transfer between HCN and Li@TAS in both tested configurations, measuring 36 me and 28 me, respectively. Overall, the study concludes that lithium-decorated TAS is a promising candidate for effectively detecting HCN gas

1. Introduction

The identification and monitoring of hazardous gases have become increasingly vital in modern industrial and environmental settings due to the significant risks they pose to human health and safety [1]. Among these harmful gases, hydrogen cyanide (HCN) is particularly notable for its high toxicity and potential for severe health impacts [2]. HCN is a colorless gas with a characteristic bitter almond odor, although it is important to note that not everyone has the genetic ability to detect this smell [3]. This compound is widely used in various industrial applications, including the manufacturing of plastics, dyes, and pesticides. Additionally, it can be released during the combustion of certain materials such as wool, silk, and synthetic polymers, further contributing to its presence in industrial and accidental fire scenarios [4]. The toxicity of HCN arises from its interference with

* Corresponding author E-mail: narkulovodil@gmail.com
https://doi.org/10.22034/crl.2026.563279.1742

cellular respiration. Specifically, it binds to cytochrome c oxidase in the mitochondria, disrupting the electron transport chain and effectively inhibiting the cell's ability to utilize oxygen [4]. This biochemical disruption leads to the rapid onset of symptoms, which can range from headache, dizziness, and nausea to more severe outcomes such as respiratory failure and death in cases of significant exposure [5]. The critical importance of detecting HCN gas cannot be overstated, particularly in environments where the risk of exposure is heightened, such as manufacturing facilities, research laboratories, and firefighting operations [5]. Early detection plays a pivotal role in preventing poisoning incidents by enabling timely evacuation or intervention. Implementing effective detection strategies is therefore essential for protecting workers' safety and minimizing the risk of accidental exposure [6]. To address the need for HCN detection, several advanced analytical methods have been developed. Techniques such as gas chromatography coupled with mass spectrometry (GC-MS), Fourier-transform infrared (FTIR) spectroscopy, and photoionization detectors (PID) are commonly employed for the precise detection and quantification of HCN gas [7]. However, these methods are often associated with notable limitations. They tend to be time-consuming, require expensive instrumentation, and demand skilled personnel for operation and maintenance. These drawbacks can hinder their practicality in certain contexts where rapid or on-site measurements are necessary. In contrast, electrochemical gas sensors have emerged as a promising alternative for HCN detection. These sensors offer several advantages over traditional analytical techniques, including simplicity, portability, cost-effectiveness, rapid response times, high sensitivity, and reliable accuracy [8]. As a result, electrochemical sensors represent an efficient and practical solution for real-time monitoring of HCN in various settings. Their adoption could significantly enhance safety measures by providing timely alerts and enabling swift actions to mitigate risks associated with this highly toxic gas. Therefore, investigating the adsorption behavior of pollutant gases on various adsorbent materials is essential for the development of effective systems for pollution control and environmental monitoring, and it plays a crucial role in protecting human health and the environment [9, 10].

Triazasumanene (TAS), a fascinating nitrogen-doped polycyclic aromatic hydrocarbon, has emerged as a promising nanostructure in the field of advanced material science due to its unique physicochemical properties and versatile applications [11]. Its distinct molecular architecture, characterized by a bowl-shaped structure with three nitrogen atoms strategically incorporated into the aromatic framework, imparts remarkable stability, electron-donating capabilities, and enhanced reactivity [12]. These features make TAS an attractive candidate for various applications, particularly in the realm of environmental monitoring and gas sensing technologies. The detection of toxic gases, is a critical challenge in ensuring public safety and environmental sustainability [13]. Conventional gas sensors often suffer from limitations such as low sensitivity, poor selectivity, and high energy consumption [14]. TAS addresses these challenges through its high surface area, excellent adsorption properties, and strong interaction with gas molecules, enabling the development of highly sensitive and selective sensors [15]. Furthermore, its ability to undergo reversible electron transfer processes enhances its responsiveness to trace concentrations of toxic gases, making it a valuable material for real-time monitoring applications [16]. Additionally, its chemical robustness and thermal stability ensure long-term operational reliability under varying environmental conditions [17].

Density Functional Theory (DFT) has established itself as an essential and highly versatile computational method in the investigation of nanostructured materials, particularly for applications in gas sensing technologies. This powerful theoretical approach offers a detailed understanding of the electronic structure and atomic-level interaction mechanisms, enabling researchers to predict and optimize material properties tailored for specific functional requirements. In this context, DFT has proven invaluable in advancing the design and performance evaluation of materials used in gas detection systems [18]. Specifically, this study employed DFT simulations to examine the gas sensing capabilities of pristine and lithium-decorated TAS nano-adsorbents, focusing on their potential as effective sensors for detecting hydrogen cyanide (HCN). Through these computational analyses, insights were gained into the adsorption behavior, electronic interactions, and overall performance of these materials, paving the way for their potential application in highly sensitive and selective gas detection technologies.

2. Materials and Methods

The research concentrated on the meticulous geometry optimization of TAS molecules, utilizing the GAMESS computational software [19] and applying the B3LYP-D3(BJ)/6-311G(d,g) basis set within a gaseous environment [20]. This initial step was critical in refining the structural configuration of TAS molecules, laying a robust foundation for subsequent analyses and investigations. The study further delved into structural modifications by introducing lithium ions into the TAS framework, resulting in the formation of Li@TAS configurations. These modified structures were analyzed both independently and in combination with an HCN molecule to gain an in-depth understanding of molecular interactions and structural adaptations. The B3LYP-D3(BJ) functional was specifically chosen due to its proven reliability and effectiveness in modeling molecular systems, as evidenced by its successful

application in prior theoretical studies [20]. Similarly, the 6-311G(d,g) basis set [21], widely recognized for its utility in molecular optimization, was employed to ensure precise and accurate results. Following the initial optimization, all configurations underwent additional refinement using the same B3LYP-D3(BJ)/6-311G(d,g) basis set [22], a step deemed essential for achieving the most stable and energetically favorable configurations, including TAS, Li@TAS, S2, and S3 [22]. In addition to structural optimization, the study also focused on evaluating the adsorption energy (Eads) of HCN gas on both pristine TAS surfaces and those modified with lithium ions. This parameter serves as a critical metric for assessing the level of attraction between gas molecules and the adsorbent surface. By quantifying the energy required for gas molecules to adhere to the adsorbent, Eads provides valuable insights into the adsorption capacity and efficiency of different adsorbents. Such measurements are instrumental in understanding the reactivity and suitability of various surfaces for molecular interactions. The calculation of Eads was performed using a specific mathematical formula, referred to as equation 1 in the study, which ensures precise and reliable quantification of adsorption energies [23-25]. These findings contribute significantly to advancing knowledge in molecular interaction dynamics and optimizing adsorbent materials for potential applications.

$$Eads = E(complex) - E(gas) - E(adsorbent) + EBSSE \quad (1)$$

In the detailed exploration of the interaction mechanisms between hydrogen cyanide (HCN) gas and an adsorbent material, we conduct a thorough calculation of the total energy of the resulting complex, referred to as E(complex). This computation is a pivotal step in deciphering the nature of the interaction and requires an in-depth assessment of the energies associated with each individual component involved in the process. Specifically, we analyze E(gas), which denotes the energy of the HCN gas molecule, and E(adsorbent), which represents the energy of the isolated adsorbent material [26]. The adsorbent in this context may either be TAS or its lithium-doped counterpart, Li@TAS. One of the significant challenges encountered during these calculations is the basis set superposition error (BSSE), which arises due to the overlapping of basis functions when the interacting components come into proximity. To address and minimize this error, we utilize the counterpoise method, a widely recognized and reliable approach that improves the accuracy of energy calculations by compensating for BSSE effects.

In addition to energy calculations, we perform a natural bond orbitals (NBO) charge analysis to gain a deeper understanding of the electronic structure and charge distribution within the molecular system [27]. This sophisticated analytical method assigns charges to individual atoms based on the occupancy of natural orbitals, providing a more precise and nuanced depiction of charge distribution compared to traditional electrostatic potential methods. By aggregating contributions from each natural orbital, weighted by their respective occupancies, NBO charge analysis offers valuable insights into molecular properties such as bond orders, bond lengths, and dipole moments. This level of detailed analysis not only enhances our ability to predict chemical behavior but also enables us to evaluate the relative stability of different molecular conformations [28]. Additionally, an important parameter in this study is the energy gap (E_g), which is defined as:

$$Eg = ELUMO - EHOMO \quad (2)$$

The concepts of E_{LUMO} and E_{HOMO} are fundamental for comprehending the energy levels associated with molecular orbitals and their implications in molecular behavior and reactivity [29]. Specifically, E_{LUMO} represents the energy of the lowest unoccupied molecular orbital, while E_{HOMO} corresponds to the energy of the highest occupied molecular orbital. These energy parameters serve as critical indicators for determining the electronic properties, chemical stability, and reactivity of molecules, making them essential tools in molecular chemistry and material science [30]. In a detailed investigation, researchers conducted analyses on both the total density of states (TDOS) and the partial density of states (PDOS) under two distinct conditions: one involving the pristine, unaltered material, and the other examining the material after it had been modified through the incorporation of a lithium atom [31]. Additionally, these evaluations extended to include the complexes formed when these materials interacted with hydrogen cyanide (HCN) gas. To further explore and quantify the interaction mechanisms between the adsorbent material and HCN gas, the electron transfer number, denoted as ΔN, was calculated [32]. This parameter is instrumental in measuring the fractional electron transfer from the complex formed between the adsorbent and HCN gas to the HCN molecule itself. Such calculations provide critical insights into the molecular-level interactions and are invaluable for understanding adsorption phenomena. Moreover, these findings hold significant implications for practical applications in areas such as gas sensing technologies, separation processes, and environmental monitoring systems, where understanding and optimizing adsorption behaviors are of paramount importance.

$$\Delta N = \frac{\mu_{HCN} - \mu_{Complex}}{2(\eta_{HCN} + \eta_{Complex})} \quad (3)$$

In the field of chemical thermodynamics, the notations μHCN and μcomplex are employed to represent the chemical potentials of hydrogen cyanide (HCN) gas and a specific complex, respectively. These chemical potentials play a fundamental role in elucidating the interactions and behaviors of substances at the molecular level. Complementing these symbols are ηHCN and

ηcomplex, which correspond to the chemical hardness of HCN and the complex. Chemical hardness is a parameter that measures a molecule's resistance to alterations in its electron distribution, providing insight into its stability and reactivity. The concept of charge transfer is particularly significant in this context [32]. When the value of ΔN, which quantifies the change in electron density between interacting species, is negative, it indicates that electrons are transferred from the complex to HCN. This scenario reveals that the complex acts as an electron donor. Conversely, a positive ΔN value implies that electrons are transferred from HCN to the complex, demonstrating that the complex functions as an electron acceptor [33]. Addressing these electron dynamics is critical for understanding molecular interactions. A notable challenge arises within density functional theory (DFT), a powerful computational framework widely used to examine van der Waals (vdW) forces. These forces, though weak, are crucial in numerous physical and biological systems, influencing processes ranging from molecular adhesion to protein folding [34]. One of the primary difficulties in DFT is achieving accurate calculations of energy dissipation, which is essential for predicting how vdW forces impact molecular behavior. To overcome this challenge, researchers frequently utilize the reduced density gradient, a sophisticated mathematical tool designed to facilitate the analysis of non-covalent interactions. Non-covalent interactions are vital for understanding how molecules interact and bind without forming strong covalent bonds typically associated with chemical reactions [35]. The reduced density gradient thus serves as an invaluable resource for investigating the nuanced yet impactful effects of vdW forces and other non-covalent interactions across diverse chemical systems.

$$RDG = 1/(2(3\pi^2)^{\frac{1}{3}} \times \frac{\nabla p}{\rho^{\frac{4}{3}}} \quad (4)$$

In the field of molecular chemistry, the symbol ρ represents the electron density distributed across a molecule, serving as a fundamental parameter in understanding molecular structure and behavior. While density functional theory (DFT) has proven to be a robust and widely used computational method for analyzing electron density, it exhibits certain limitations in accurately identifying and characterizing specific non-covalent interactions, such as hydrogen bonding, van der Waals forces, and steric repulsion. To overcome these challenges, researchers have turned their attention to the electron density Hessian matrix, with a particular focus on the sign of its second largest eigenvalue, denoted as λ2 [36]. This eigenvalue provides crucial insights into the nature and strength of non-covalent interactions. The expression Ω = sign(λ2)ρ is particularly useful in classifying these interactions, as the sign of λ2 reflects key information about the interaction's characteristics based on the electron density distribution. To further enhance the understanding and visualization of these interactions, the Reduced Density Gradient (RDG) method is applied within the framework of non-covalent interaction (NCI) theory [37]. This method enables scientists to generate detailed visual representations of non-covalent forces using advanced graphical techniques. The MULTIWFN39 software package plays an indispensable role in this analytical process by facilitating the creation of scatter plots between relevant functions and producing cube files that are critical for in-depth analysis. Additionally, visualization is significantly improved through the use of VMD software, which allows researchers to generate color-filled isosurface graphs. These visual tools provide an intuitive and detailed depiction of the complex molecular interactions, offering deeper insights into the dynamics and behavior of molecules at an atomic level [38].

3. Results and Discussion

3.1. Geometry optimization of TAS and HCN

The structure of TAS, as demonstrated in Figure 1, consists of a total of 18 carbon atoms and three nitrogen atoms, forming a nanosheet-like configuration that exhibits a subtle curvature with an angle of 155°. This structural arrangement includes various types of carbon-carbon (C–C) bonds with differing lengths, which are specifically associated with the carbon atoms located within the pentagonal and hexagonal rings, as shown in Figure 1a. A detailed investigation into the electronic properties of TAS has been performed, focusing particularly on its molecular orbital energies. The corresponding energy values for the highest occupied molecular orbital (HOMO), the lowest unoccupied molecular orbital (LUMO), and the energy gap (Eg) are systematically presented in Table 1. Additionally, the total density of states (TDOS) for TAS, which reveals an energy gap of 4.22 electron volts (eV), is graphically depicted in Figure 1c. These results are consistent with findings reported in previous studies, further validating the accuracy of the current analysis. For comparison, Figure 1b illustrates the optimized molecular structure of HCN, providing a contrasting perspective on molecular configurations and emphasizing the unique characteristics of TAS.

3.2. Adsorption of HCN on the pristine TAS

In the quest to comprehend the adsorption properties of hydrogen cyanide (HCN) on TAS surfaces, an array of preliminary configurations was assessed. These configurations involved aligning the hydrogen and nitrogen terminals of HCN either directly above the core of the pentagonal ring or near a carbon atom. This methodology aimed to pinpoint the configuration that would result in the lowest adsorption energy across both the internal and external surfaces of the adsorbent. During

the optimization phase, modifications were made to the orientation of HCN, specifically adjusting its hydrogen atom closer to a nitrogen atom within the pentagonal ring structure of TAS. Following the completion of geometric optimization, it was found that only two configurations, named S1 and S2, demonstrated stability, as illustrated in Figures 2a and 2b. The adsorption energy, Gibbs free energy changes (ΔG_{ads}), enthalpy changes (ΔH_{ads}), charge polarization (QT), and dipole moments were thoroughly examined and are summarized in Table 1. The computed adsorption energy (E_{ads}) for the S1 configuration, derived using equation 1, is documented in Table 1. The Eads values for S1 and S2 were calculated to be -5.88 and -1.57 kcal mol^{-1}, respectively, indicating a very weak physical adsorption, which is energetically unfavorable. The enthalpy change (ΔH_{ads}) and Gibbs free energy change (ΔG_{ads}) were determined to be -5.08, 2.15 kcal mol^{-1} and -1.33 and 5.69 kcal mol^{-1} for S1 and S2 conformers, respectively, further demonstrating that the adsorption process is thermodynamically unfavorable. The distance between carbon and hydrogen atoms in the S2 configuration was measured to be 2.06 Å, as shown in Figure 2a, while the distance between carbon and nitrogen atoms was measured to be 2.61 Å, as shown in Figure 2b. According to the data presented in Table 1, HCN gas adsorption on TAS surfaces in both configurations is accompanied by a partial charge transfer, with approximately −32 and 2 |me| for S1 and S2 conformers being transferred from the nano-adsorbent to the gas.

The results suggest that there is a weak electrostatic interaction between HCN and TAS, indicating that unmodified TAS is not an effective sensor for detecting or identifying HCN gas [23-25].

The electronic properties of both configurations were rigorously evaluated to gain a comprehensive understanding of the influence of HCN adsorption on the pristine TAS's electronic characteristics. As detailed in Table 2, the adsorption process induces a subtle shift in both the energy gap (Eg) and the Fermi level (EFL). Specifically, the energy gap values for the S1 and S2 configurations were calculated to be 4.34 eV and 4.31 eV, respectively.

This minor variation in the percentage change of the energy gap (% ΔEg) is attributed to the weak adsorption interaction occurring on the outer surface of the pristine TAS [26]. To further elucidate these findings, the Total Density of States (TDOS) was analyzed in depth and is graphically represented in Figure 2b. The results indicate that there is no significant alteration in the TDOS profile between the S1 configuration and the original TAS structure. Additionally, the electron transfer number (ΔN) was computed to evaluate electron deflection tendencies, which are influenced by electrical and chemical potential parameters [27].

This deflection tendency is closely related to the ease with which electron density can be redistributed and is determined by the size of the involved ions and atoms. Importantly, the ΔN values at the adhesion sites were found to be negative, signifying electron transfer from TAS to HCN. These findings align with the Natural Bond Orbital (NBO) analysis results, which confirm a charge transfer of −32 and 2 |me| from HCN to TAS for S1 and S2 conformers, as summarized in Table 2 [28].

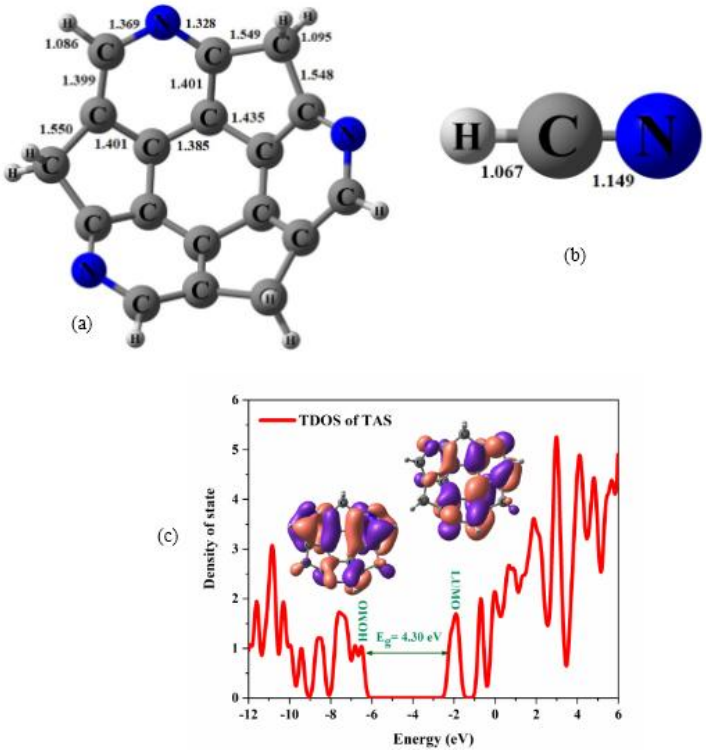

Fig. 1. Optimized structure of (a) TAS (b) HCN gas, (c) total density of states (TDOS) of TSSUM (All distances are in Å).

Table 1. Dipole moment, charge polarization transfer from nanostructure to gas molecule (QT) and adsorption energy (E_{ads}) and calculated thermodynamic properties at 298K and 1atm (ΔH_{ads} and ΔG_{ads}) of TAS, S1 and S2 configurations.

Systems	Dipole moment	Q_T (me)	E_{ads} (kcal/mol)	ΔH_{ads} (kcal/mol)	ΔG_{ads} (kcal/mol)
HCN	3.06	-	-	-	-
TAS	2.11	-	-	-	-
S1	6.99	-32	-5.88	-5.08	2.15
S2	3.15	2	-1.57	-1.33	5.69

Table 2. Energy of HOMO and LUMO orbitals, energy difference of HOMO and LUMO orbitals (E_g), Fermi level energy (EFL), the change of energy gap of nanocone after adsorption(ΔE_g(%)), working function (Φ), the change of working function of nanocone after adsorption (ΔΦ), electron transfer number (ΔN), chemical potential (μ), hardness (η), and electrophilicity (ω) for HCN molecule, Triazasumanene (TAS), S1, and S2 configurations at the theoretical level of B3LYP-D3(BJ)/6-311G(d,g).

Systems	E_{HOMO} (eV)	E_{FL} (eV)	E_{LUMO} (eV)	E_g (eV)	%ΔE_g	Φ (eV)	ΔΦ (eV)	ΔN	μ (eV)	η (eV)	ω (eV)
HCN	-10.20	-5.22	-0.24	9.96	-	5.22	-	-	-5.22	4.98	2.74
TAS	-6.48	-4.33	-2.18	4.30	-	-4.33	-	-	-4.33	2.15	4.35
S1	-6.81	-4.64	-2.47	4.34	0.66	-4.64	0.31	-0.04	-4.64	2.16	4.97
S2	-6.33	-4.17	-2.02	4.31	0.19	-4.17	-0.16	-0.07	-4.17	2.15	4.04

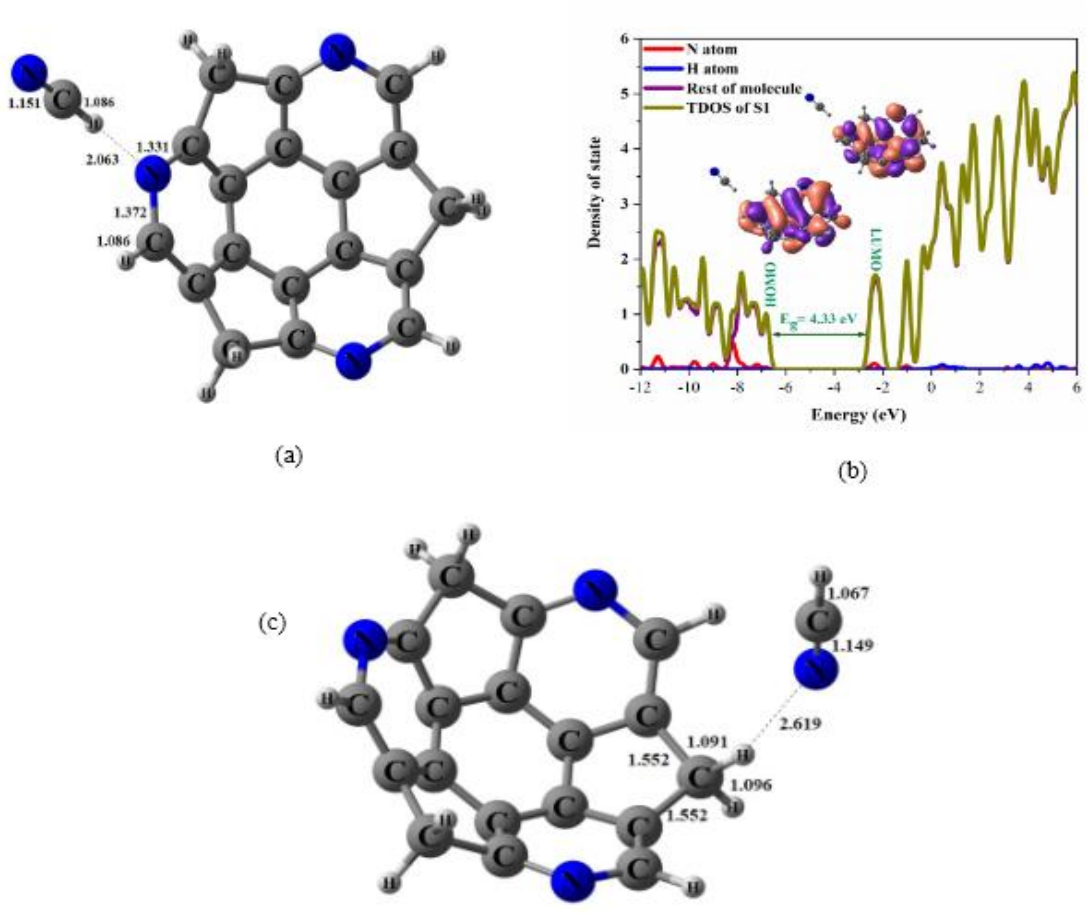

Fig. 2. (a), (c) Optimized structure, (b) total density of states (TDOS) and partial density of state (PDOS) of S1, S2 configuration (All distances are in Å).

Furthermore, altering the work function of materials represents a pivotal strategy for optimizing electronic device performance. The work function of nanomaterials plays a critical role in controlling their surface properties, and in this study, the variations in work function due to charge transfer between pristine TAS and HCN were meticulously investigated to provide deeper insights into these interactions and their implications for material performance. The work function is a fundamental concept in the field of solid-state physics, describing the minimum energy required to remove an electron from the Fermi level of a material and transfer it to a position just outside the material's surface into the vacuum. This energy barrier is crucial for understanding various electron emission processes and plays a significant role in applications such as thermionic emission,

photoemission, and field emission. Represented by the symbol Φ, the work function is typically measured in electron volts (eV), providing a quantitative measure of the energy threshold. The study of electron emission processes often involves analyzing the current density, which quantifies the flow of electrons per unit area into the vacuum. This parameter is essential for characterizing the efficiency and behavior of electron emission in different materials, thereby contributing to advancements in technologies like vacuum electronics, electron microscopy, and semiconductor devices. Understanding the work function and its implications allows scientists and engineers to design materials and systems optimized for specific applications, emphasizing its importance in both theoretical studies and practical innovations. The current density, j, can be calculated using the formula:

$$j = AT^2 \exp\left(-\frac{\Phi}{KT}\right) \quad (5)$$

The variable A denotes Richardson's constant, which has units of amperes per square meter (A m^{-2}). T refers to the absolute temperature measured in Kelvin (K), and K represents Boltzmann's constant, a fundamental physical constant. This relationship is derived from the Richardson-Dushman equation, a key formula in the study of thermionic emission. Thermionic emission describes the phenomenon where electrons are emitted from the surface of a material when it is heated to high temperatures. This process is crucial in understanding various applications, such as vacuum tubes, electron guns, and certain types of sensors. The Richardson-Dushman equation provides a quantitative framework for predicting the current density of emitted electrons based on material properties and temperature conditions, making it an essential tool in fields like condensed matter physics and electronic engineering. To compute the work function, the following equation was employed:

$$\Phi = \text{Einf} - \text{EFL} \quad (6)$$

In this particular equation, the term E_{FL} refers to the energy level of electrons at the Fermi level, which represents the highest energy state that electrons can occupy under conditions of absolute zero temperature. Essentially, it serves as a critical reference point for describing the electronic properties of a material. Meanwhile, E_{inf} denotes the electrostatic potential at infinity, which is often simplified by assuming it to be zero in order to streamline calculations. This assumption does not impact the overall validity of the analysis but rather facilitates a more straightforward interpretation of the results. The calculation of these parameters plays a significant role in providing a deeper understanding of the energy landscape experienced by electrons within a given material. Specifically, it sheds light on their capacity to overcome the potential energy barrier present at the material's surface. Such insights are of paramount importance when determining or manipulating the work function, a property that is central to numerous technological applications.

For instance, in electronic devices such as cathodes used in vacuum tubes and electron microscopes, precise control over electron emission is essential for ensuring optimal performance and functionality. Therefore, mastering the concepts and calculations related to the work function is indispensable in advancing innovations in these and other related fields [28-30]

The interaction between TAS and HCN, along with the corresponding work function values, is comprehensively presented in Table 2, derived using Density Functional Theory (DFT) calculations. Notably, the work function values of pristine TAS undergo measurable changes upon the adsorption of HCN molecules onto its surface. As described by equation (4), the electron diffusion current density exhibits an exponential dependence on the negative work function. However, despite the adsorption process, no significant shifts were observed in the work function or Fermi level of TAS. This resulted in only a gradual increase in current density following the adherence of HCN to the outermost layer of TAS, highlighting a limited sensitivity of the adsorbent material to HCN molecules. The calculated ΔΦ values for the S1 and S2 conformers further suggest that pristine TAS holds potential as a type-4 sensor due to its relatively low adsorption energy [31-33]. Additionally, the interaction between HCN and TAS induces modifications in the electronic structure of TAS, which can be observed through changes in its electrical conductivity. This behavior underscores the potential application of TAS in sensing technologies while providing insight into its electronic response to HCN exposure. The conduction electron population of semiconductors, which is responsible for electrical conductance, was computed to further understand these changes with the following equation:

$$s = AT3/2 \exp(-Eg/2kT) \quad (7)$$

In the realm of chemical sensors, the parameter denoted as A, expressed in units of electrons per cubic meter per Kelvin raised to the power of three over two, serves as a fundamental constant that significantly influences the operational mechanisms of these devices. Furthermore, the constant k represents Boltzmann's constant, a pivotal physical constant essential for a wide range of thermodynamic computations. As highlighted earlier, the functionality of chemical sensors is primarily based on their ability to detect changes in electrical conductance, which arise due to the adhesion process. This process entails interactions between the sensor's surface and the targeted chemical species, resulting in modifications to the sensor's electrical properties. A prior investigation, specifically referenced as study number [34], has provided valuable insights into this phenomenon, demonstrating that the relationship

between adhesion-induced conductance variations and sensor performance can be effectively leveraged to evaluate the sensitivity of these devices. Notably, it has been shown that fluctuations in the energy gap, symbolized as Eg, serve as a critical indicator of the sensor's responsiveness and sensitivity.

By meticulously studying these variations, researchers and developers are able to derive meaningful conclusions regarding the efficiency and accuracy of chemical sensors. This knowledge is instrumental in refining sensor designs and optimizing their applications across diverse domains, including environmental monitoring, industrial safety protocols, and healthcare diagnostics, thereby contributing to advancements in these critical fields.

3.3. Adsorption of HCN on the Li@TAS

In recent years, there has been the development of an innovative and highly effective strategy aimed at improving the interaction between adsorbing molecules and host adsorbents, which has opened new avenues in the field of adsorption technologies. This novel approach involves the deliberate decoration or modification of adsorbents using a variety of elements, including alkali metals, alkaline earth elements, group III elements, and transition metals [35]. The incorporation of these elements onto the adsorbent's surface has proven to be a groundbreaking advancement, as it significantly enhances the adsorbent's ability to interact with target molecules. This decorating strategy is typically executed through the use of functional groups that exhibit the capacity to interact with the adsorbent's surface via multiple mechanisms. These mechanisms include, but are not limited to, hydrogen bonding, electrostatic interactions, van der Waals forces, and other molecular-level interactions that facilitate a closer and more effective binding between the adsorbent and the adsorbing molecule [36]. Additionally, the surface of the adsorbent itself can be further tailored or modified to maximize its interaction potential. One method to achieve this is by increasing the number of active or accessible sites available for adsorption. This can be accomplished through the incorporation of various chemical components such as polymers, surfactants, and functional groups that exhibit either hydrophilic or hydrophobic properties, depending on the specific requirements of the adsorption process [37]. By introducing these modifications, the adsorbent's surface becomes more versatile and capable of interacting with a wider range of molecules under varying environmental conditions. The combination of increasing accessible sites and reinforcing the strength of interactions between adsorbing molecules and the host adsorbent ultimately leads to a substantial improvement in the overall efficiency and performance of the adsorption process [38].

To enhance the adsorption energy of TAS and establish it as an effective gas sensor for detecting hydrogen cyanide (HCN), a targeted decoration strategy was employed. This method not only increased the adsorption capacity but also significantly improved the sensitivity and selectivity of the adsorbent, positioning it as a highly effective tool for gas sensing applications. The study focused on strategically modifying the central benzene ring of the original TAS molecule, both on its internal and external surfaces, by incorporating lithium (Li) metal. This modification aimed to explore how such alterations could influence the structural and electronic properties of the TAS compound.

Following this approach, the newly designed structures underwent optimization, and their electronic properties were carefully analyzed to assess any notable changes in performance. The optimized configurations of the Li-decorated TAS compounds, referred to as Li@TAS-1 for internal surface decoration and Li@TAS-2 for external surface decoration, are illustrated in Figure 3 of the study. A significant observation was the average distance between carbon and lithium atoms, which ranged from 1.360 to 2.442 Å in Li@TAS-1 and from 1.386 to 2.483 Å in Li@TAS-2, indicating a stable interaction that could potentially be fine-tuned to meet specific application needs. A comprehensive analysis of the electronic properties of these structures was conducted, with key parameters such as E_{HOMO}, E_{LUMO}, E_{FL}, and Eg systematically evaluated and presented in Table 3. The results revealed a substantial transformation in the Eg values of both Li@TAS-1 and Li@TAS-2 compared to pristine TAS, with notable shifts in HOMO and LUMO energy levels toward lower states. This led to reduced Eg values of 1.64 eV for Li@TAS-1 and 1.49 eV for Li@TAS-2, underscoring the potential of these modified structures for enhanced gas sensing performance.

The study further explored the adsorption behavior of hydrogen cyanide (HCN) on the Li@TAS-1 and Li@TAS-2 structures, with a particular focus on the regions where lithium decoration occurs. This investigation aimed to provide a deeper understanding of how lithium decoration influences interaction dynamics with other molecules, thereby offering valuable insights into potential applications of the modified TAS compounds. The findings of this analysis are presented in Figures 4(a–d), which illustrate the interaction between the nitrogen atom of HCN gas and the lithium atom in the Li@TAS-1 and Li@TAS-2 structures. To quantify the adsorption energy, Eads values for the resulting configurations were calculated using equation (1), with the results summarized in Table 4. Two stable configurations were identified: configuration S3, depicted in Figure 4a, where the nitrogen atom of HCN gas interacts with Li@TAS-1, and configuration S4, shown in Figure 4c, where the nitrogen atom of HCN gas

engages with Li@TAS-2. The adsorption energies (Eads) for configurations S3 and S4 were found to be −12.24 and −22.31 kcal mol−1, respectively, confirming the chemical adsorption of HCN gas onto the Li@TAS-1 and Li@TAS-2 surfaces. These results demonstrate that HCN gas molecules can form strong bonds with Li@TAS structures, thereby contributing to the stability of these configurations.

This study examines the interaction between nitrogen from HCN gas and lithium from Li@TAS-1 and Li@TAS-2 adsorbents. The interaction distances are approximately 1.931 Å and 1.991 Å in the S3 configuration and 1.965 Å in the S4 configuration on the surfaces of Li@TAS-1 and Li@TAS-2, respectively. These distances suggest chemical adsorption occurs between the two elements in both adsorbents. The interaction distances, along with adsorption energy values, indicate that both configurations are highly favorable for HCN adsorption.

Thermodynamic parameters further support this conclusion, with ΔGads and ΔHads values of -12.87 kcal mol−1 and -22.54 kcal mol−1 for S3, and -13.65 kcal mol−1 and -21.51 kcal mol−1 for S4, respectively, demonstrating thermodynamic favorability in both configurations. NBO analysis highlights a significant charge transfer following adsorption, with 36 |me| transferred from HCN gas to Li@TAS-1 and 28 |me| to Li@TAS-2, indicating strong bond formation driven by electron exchange, which elevates the energy state of the combined molecules. Further investigation into electronic properties, including E_{HOMO}, E_{LUMO}, and the energy gap (Eg), reveals notable changes in Eg for S3 and S4 compared to the pristine Li@TAS-1 and Li@TAS-2 adsorbents, with reductions of 7.70% and 8.38%, respectively. This suggests a pronounced adsorptive and electronic response to HCN gas, with new HOMO and LUMO levels for S3 and S4 being lower than those of Li@TAS-1 and Li@TAS-2, leading to substantial changes in Eg.

These findings imply that Li@TAS materials exhibit sufficient sensitivity for HCN gas detection. Analysis of ΔN values for S3 and S4 configurations reveals negative values of -0.23 and -0.21, confirming electron transfer from HCN gas to the Li@TAS adsorbents. Additionally, examination of ΔΦ values indicates a negative shift in ΔΦ for both configurations, resulting in a reduced work function (Φ) compared to the pristine Li@TAS-1 and Li@TAS-2 adsorbents.

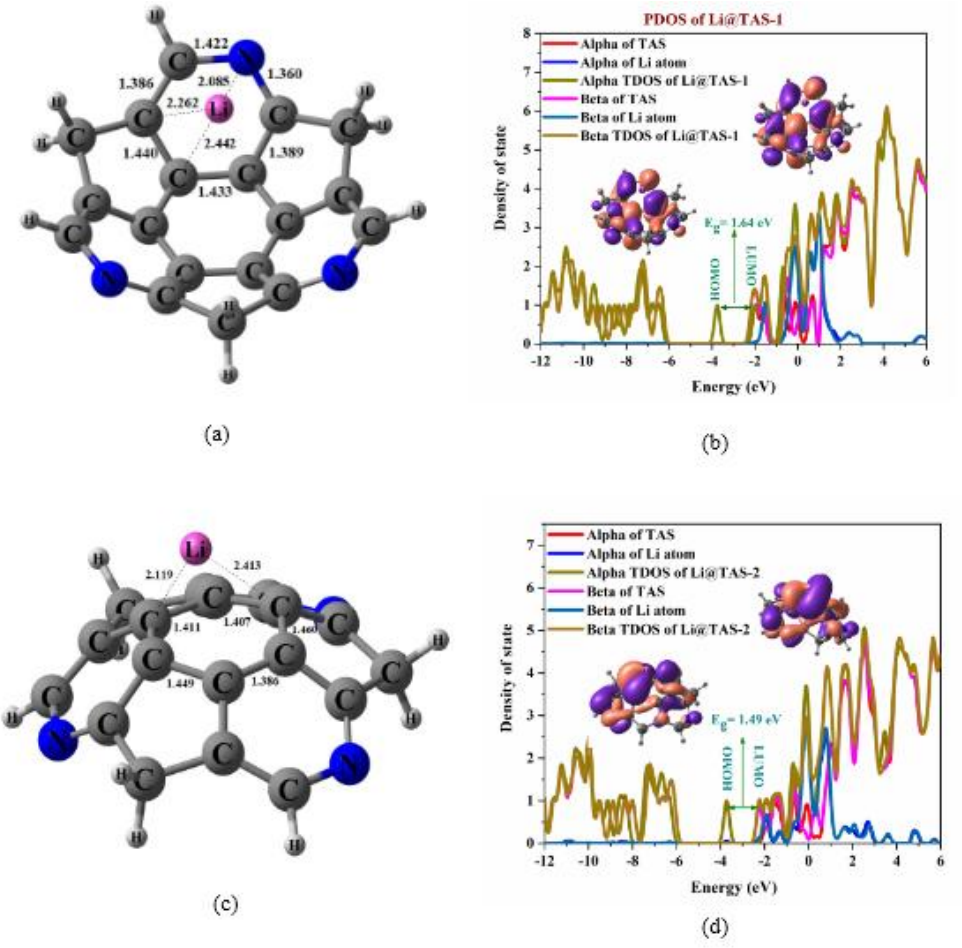

Fig. 3. (a), (c) Optimized structures, (b), (d) total density of states (TDOS) and partial density of state (PDOS) of Li@TAS-1 and Li@TAS-2 configurations (All distances are in Å).

Table 3. Energy of HOMO and LUMO orbitals, energy difference of HOMO and LUMO orbitals (E_g), Fermi level energy (E_{FL}), the change of energy gap of nanocone after adsorption(ΔE_g(%)), working function (Φ), the change of working function of nanocone after adsorption (ΔΦ), electron transfer number (ΔN), chemical potential (μ), hardness (η), and electrophilicity (ω) for HCN molecule, lithium decorated Triazasumanene (Li@TAS-1 and Li@TAS-2), S3 and S4 configurations at the theoretical level of B3LYP-D3(BJ)/6-311G(d,g).

Systems	E_{HOMO} (eV)	E_{FL} (eV)	E_{LUMO} (eV)	E_g (eV)	%ΔE_g	Φ (eV)	ΔΦ (eV)	ΔN	μ (eV)	η (eV)	ω (eV)
Li@TAS-1	-3.76	-2.94	-2.12	1.64	-	2.94	-	-	-2.94	0.82	5.26
S3	-3.38	-2.63	-1.87	1.51	7.70	2.63	-0.31	-0.23	-2.63	0.76	4.56
Li@TAS-2	-3.72	-2.97	-2.23	1.49	-	2.97	-	-	-2.97	0.74	5.94
S4	-3.53	-2.85	-2.17	1.36	8.38	2.85	-0.12	-0.21	-2.85	0.68	5.97

Table 4. Dipole moment, charge polarization transfer from nanostructure to gas molecule (Q_T) and adsorption energy (E_{ads}) and calculated thermodynamic properties at 298K and 1atm (ΔH_{ads} and ΔG_{ads}) of Triazasumanene (Li@TAS-1 and Li@TAS-2), S3 and S4 configurations.

Systems	Dipole moment	Q_T (me)	E_{ads} (kcal/mol)	ΔH_{ads} (kcal/mol)	ΔG_{ads} (kcal/mol)
Li@TAS-1	3.95	-	-12.24	-14.41	-7.02
S3	6.69	36	-22.54	-22.33	-12.87
Li@TAS-2	5.87	-	-7.46	-9.56	-3.30
S4	12.66	28	-22.31	-21.51	-13.65

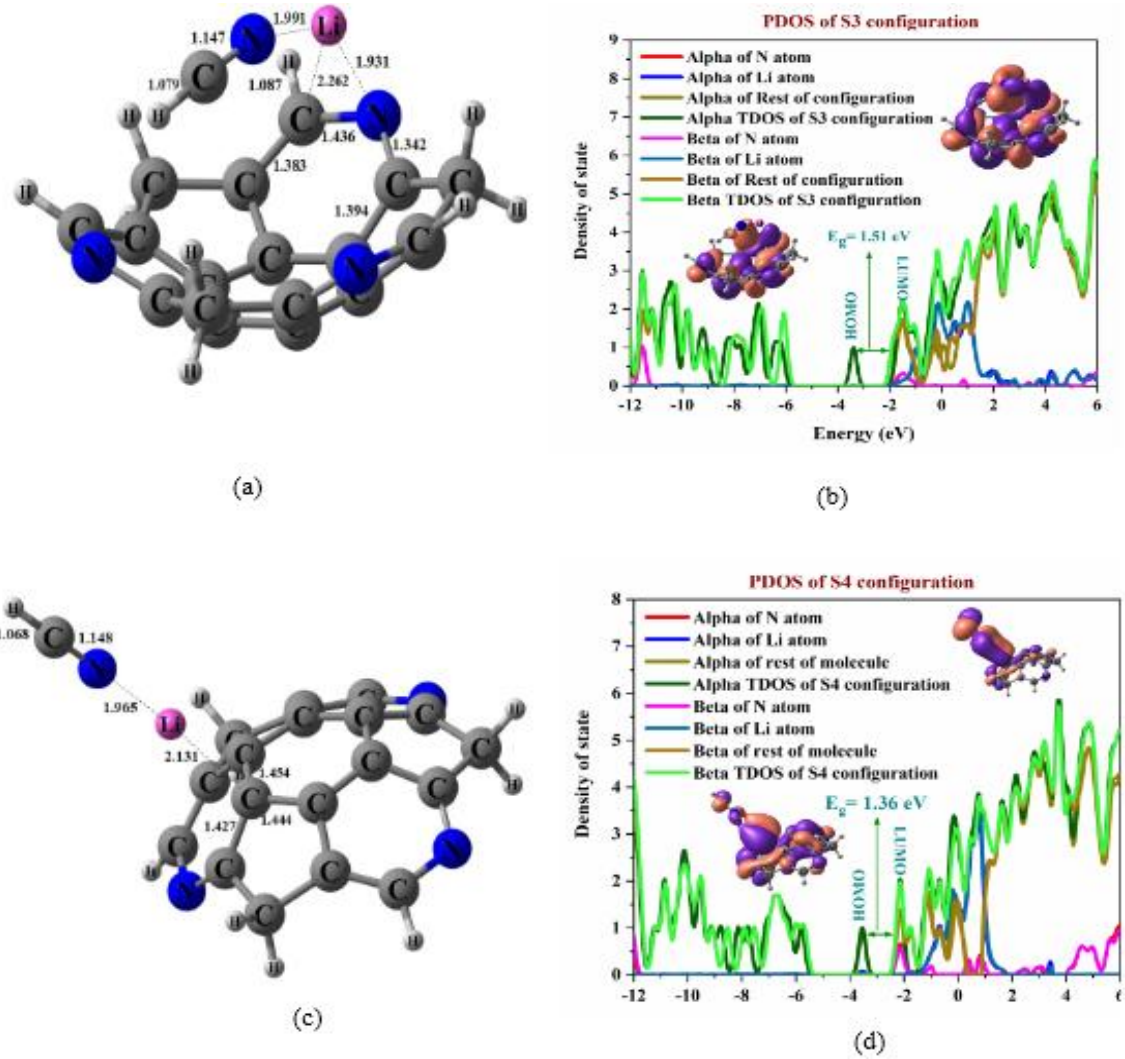

Fig. 4. (a), (c) Optimized structures, (b), (d) total density of states (TDOS) and partial density of state (PDOS) of S_3 and S_4 configurations (All distances are in Å).

3.4. Analysis of non-covalent interaction (NCI) and reduced-density gradient (RDG).

The Non-Covalent Interaction (NCI) analysis is a highly effective method for gaining detailed insights into the nature of non-covalent interactions within molecular systems. This analytical approach is particularly valuable for differentiating between weak intermolecular forces and the stronger, more localized interatomic attractions. The NCI plot utilizes a color gradient ranging from blue to green to red and operates within a defined (λ2)ρ range of −0.05 to +0.05 atomic units (au).

This carefully selected range plays a crucial role in identifying the type, intensity, and precise location of the interactions being studied. By interpreting data derived from NCI analysis, researchers can achieve a deeper understanding of the fundamental forces driving molecular interactions, which, in turn, enhances our knowledge of chemical reactivity.

For example, regions with positive (λ2)ρ values, indicative of strong repulsive non-bonded overlaps, are represented by red in graphical outputs such as Figure 5. In contrast, weaker interactions are depicted by green and blue regions, corresponding to very weak and attractive interactions, respectively. This detailed approach allows scientists to unravel and analyze the complex interplay of forces within molecular structures, advancing our comprehension of chemical phenomena. Within the context of molecular interactions analyzed using the B3LYP-D3(BJ)/6-311G(d) computational framework, intriguing patterns emerge in the scatter plots of Li@TAS-1 and Li@TAS-2 for configurations S3 and S4. The nature of HCN adsorption on the TAS surface was elucidated using reduced density gradient (RDG) analysis combined with sign(λ_2)ρ plots, as shown in Figure 5.

For the Li-decorated TAS configurations (Figure 5a and 5b), pronounced blue RDG isosurfaces appear between the Li atom and the nitrogen end of HCN, accompanied by distinct spikes in the negative sign(λ_2)ρ region. These features indicate strong stabilizing interactions, which can be attributed to electrostatic attraction and partial Lewis acid–base coordination between the positively polarized Li center and the lone pair on the N atom of HCN. In addition to this dominant interaction, green RDG regions surrounding the adsorbate and the TAS framework suggest the presence of secondary van der Waals interactions that further stabilize the adsorption complex. Among the examined structures, the S3 configuration (Figure 5c) exhibits the most intense blue isosurfaces and the strongest negative sign(λ_2)ρ contribution, implying an optimized adsorption geometry in which Li–N coordination is maximized while being supported by favorable interactions with the TAS surface. In contrast, the S4 configuration (Figure 5d) is characterized mainly by green RDG features and a weak negative sign(λ_2)ρ signal, indicating that HCN adsorption in this case is governed primarily by van der Waals forces and corresponds to a weak physisorption regime.

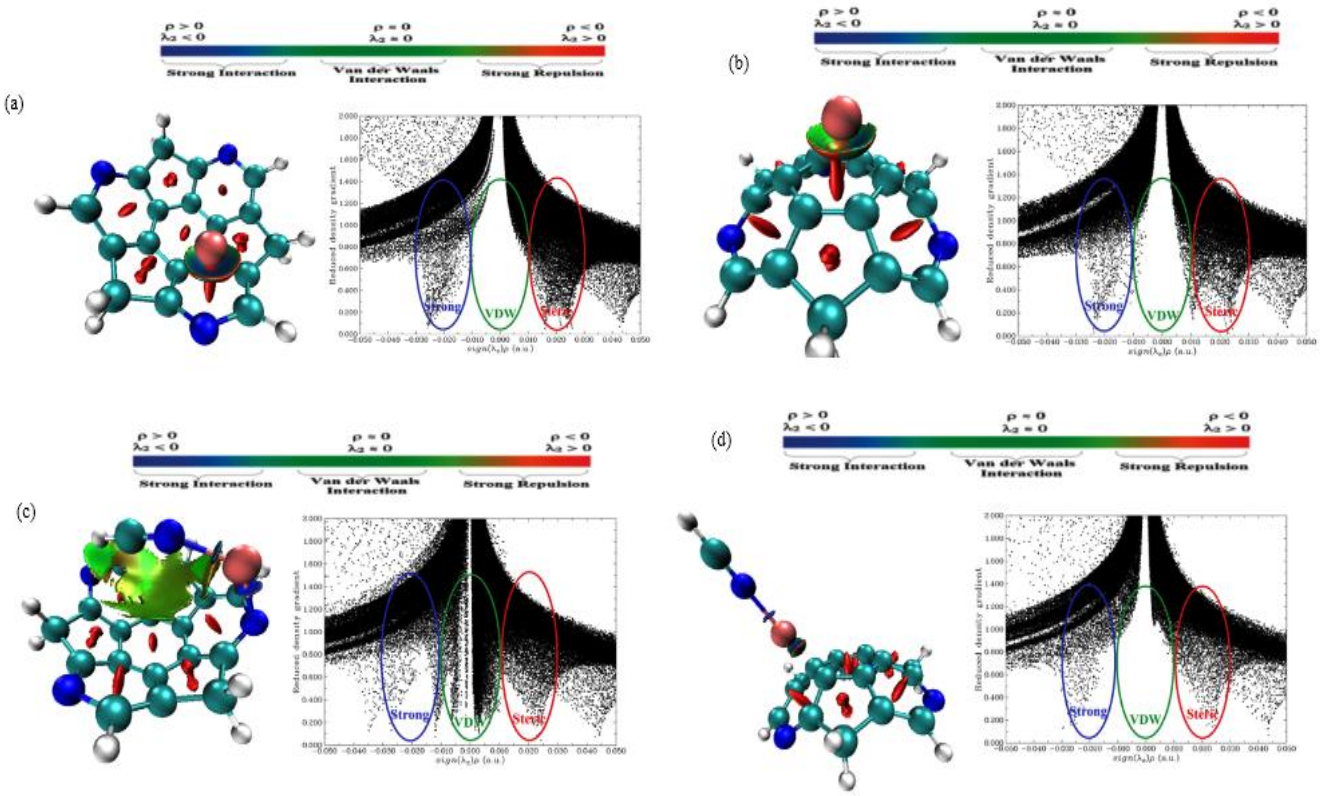

Fig. 5. Color-filled RDG isosurface maps (isovalue = 0.5 au) and plot of the reduced density gradient (RDG) versus sign (λ_2)ρ for (a) Li@TAS-1, (b) Li@TAS-1, (c) S3,and (d) S4 configurations.

Overall, these results suggest that HCN adsorption on TAS proceeds preferentially through an N-end-down orientation toward Li sites, where a synergistic combination of Li–N electrostatic/coordination interactions and dispersive forces lead to enhanced binding. This mixed chemisorption–physisorption mechanism highlights the critical role of accessible Li centers in improving the HCN capture performance of TAS-based adsorbents.

4. Conclusion

This study utilized advanced computational methods, specifically density functional theory (DFT) calculations, to evaluate the potential of Triazasumanene (TAS) nanostructures, both in their original form and enhanced with lithium atoms, as effective sensors for the detection of the hazardous hydrogen cyanide (HCN) gas. The initial findings revealed that pristine TAS exhibited only weak interactions with HCN molecules, as evidenced by minimal changes in its electronic properties, particularly its bandgap (Eg). This indicated that unmodified TAS alone was not particularly effective for HCN sensing. To address this limitation and enhance its sensitivity, the TAS structure was modified by incorporating a lithium atom, resulting in a lithium-decorated variant referred to as Li@TAS. The subsequent analysis of adsorption energy and thermodynamic parameters demonstrated that the interaction between HCN and Li@TAS was significantly stronger. The calculated negative adsorption energies indicated that the adsorption process was thermodynamically favorable, exothermic, and spontaneous under typical experimental conditions. Furthermore, a detailed density of states (DOS) analysis showed that the bandgap of Li@TAS decreased notably by 8.38%, from 1.49 eV to 1.36 eV, upon interaction with HCN, highlighting a substantial change in its electronic structure. Additional insights into the nature of the interaction were provided by non-covalent interaction (NCI) and reduced density gradient (RDG) analyses, which confirmed the formation of a strong bond between the nitrogen atom of the HCN molecule and the lithium atom on the modified TAS structure. Moreover, natural bond orbital (NBO) charge transfer analysis revealed significant charge transfer between HCN and Li@TAS in two tested configurations, with measured values of 36 me and 28 me, respectively. These findings collectively underscore that lithium modification greatly enhances TAS's ability to detect HCN gas. Consequently, the study concludes that Li@TAS is a highly promising candidate for use as an efficient sensor for monitoring the presence of hazardous HCN gas in various environments.

References

[1] J. Barcroft, The toxicity of atmospheres containing hydrocyanic acid gas. *Epidemiol. Infect.*, 31 (1931) 1-34. https://doi.org/10.1017/S0022172400010664

[2] J.O. Egekeze, F.W. Oehme, Cyanides and their toxicity: a literature review. *Vet. Q.*, 2 (1980) 104-114. https://doi.org/10.1080/01652176.1980.9693766

[3] J.H. Wolfsie, C.B. Shaffer, Hydrogen cyanide: Hazards, toxicology, prevention and management of poisoning. *J. Occup. Environ. Med.*, 1 (1959) 281-288.

[4] J.I. Lachowicz, J. Alexander, J.O. Aaseth, Cyanide and Cyanogenic Compounds—Toxicity, Molecular Targets, and Therapeutic Agents. *Biomolecules*, 14 (2024) 1420. https://doi.org/10.3390/biom14111420

[5] F.M. Esposito, Y. Alarie, Inhalation toxicity of carbon monoxide and hydrogen cyanide gases released during the thermal decomposition of polymers. *J. Fire Sci.*, 6 (1988) 195-242. https://doi.org/10.1177/073490418800600303

[6] R.Q. Wu, M. Yang, Y.H. Lu, Y.P. Feng, Z.G. Huang, Q.Y. Wu, Silicon carbide nanotubes as potential gas sensors for CO and HCN detection. *J. Phys. Chem. C*, 112 (2008) 15985-15988. https://doi.org/10.1021/jp804727c

[7] a) S.M. Zain, R. Shaharudin, M.A. Kamaluddin, S.F. Daud, Determination of hydrogen cyanide in residential ambient air using SPME coupled with GC–MS. *Atmos. Pollut. Res.*, 8 (2017) 678-685. b) Q. Zhu, W. Wang, C. Shan, Y. Xie, P. Wu, B. Liang, et al., Spatiotemporal Variations and Characteristics of CO, H2CO and HCN Emissions from Biomass Burning Monitored by FTIR Spectroscopy. *Remote Sens.*, 16 (2024) 3586. c) H.B. Singh, L. Salas, D. Herlth, R. Kolyer, E. Czech, W. Viezee, et al., In situ measurements of HCN and CH3CN over the Pacific Ocean: Sources, sinks, and budgets. *J. Geophys. Res.*, 108 (2003) D20.

[8] M.R. Jalali Sarvestani, T. Madrakian, A. Afkhami, Developed electrochemical sensors for the determination of beta-blockers: a comprehensive review. *J. Electroanal. Chem.*, 899 (2021) 115666. https://doi.org/10.1016/j.jelechem.2021.115666

[9] a) M. Patil, S.N. Mathad, A. Patil, R.S. S., R. Bakale, Understanding the Role of Natural Gas Contaminants in CO_2/CH_4 Separation Using Advanced Polyimide Membrane Technology. *J. Chem. Lett.*, 6 (2025) 181–187. b) A.B. Adam, R. Panbani, M.Y. Abubakar, Metal-Organic Frameworks (MOFs) for Explosive Gas Detection in Refineries. *J. Chem. Technol.*, 1 (2025) 31–46.

[10] a) A.S. Hessen, N.M.A. Alsultany, H. Bahir, A.H. Adthab, S. Soleimani-Amiri, S. Ahmadi, et al., Adsorption of sulfur mustard on the transition metals (TM = Ti2+, Fe2+, Co2+, Ni2+, Cu2+, Zn2+) porphyrins induced in carbon nanocone (TM-PCNC): Insight from DFT calculation. *J. Mol. Graph. Model.*, 135 (2025) 108928. b) E. Vessally, S. Soleimani-Amiri, A. Hosseinian, L. Edjlali, A. Bekhradnia, The Hartree-Fock exchange effect on the CO adsorption by the boron nitride nanocage. *Physica E*, 87 (2017) 308–311. c) S. Soleimani-Amiri, A. Khanmohammadi, E. Vessally, J. Makasana, S. Ballal, R. Panigrahi, et al., Metal–porphyrin functionalized carbon nanocones as promising $COCl_2$ sensors: a DFT and NBO perspective. *Comput. Theor. Chem.*, 1253 (2025) 115457.

[11] Q. Tan, P. Kaewmati, S. Higashibayashi, M. Kawano, Y. Yakiyama, H. Sakurai, Triazasumanene: an isoelectronic heteroanalogue of sumanene. *Bull. Chem. Soc. Jpn.*, 91 (2018) 531-7. https://doi.org/10.1246/bcsj.20170384

[12] M. Saito, H. Shinokubo, H. Sakurai, Figuration of bowl-shaped π-conjugated molecules: properties and functions. *Mater. Chem. Front.*, 2 (2018) 635-661. https://doi.org/10.1039/C7QM00593H

[13] S. Hiroto, Heteroatoms in bowl-shaped polycyclic aromatic hydrocarbons: synthesis and structures. *Chem. Lett.*, 50 (2021) 1146-1155. https://doi.org/10.1246/cl.200965

[14] X. Chen, H. Sakurai, H. Wang, S. Gao, H.D. Bi, F.Q. Bai, Theoretical study on the molecular stacking interactions and charge transport properties of triazasumanene crystals–from explanation to prediction. *Phys. Chem. Chem. Phys.*, 23 (2021) 4681-9. https://doi.org/10.1039/D0CP06102F

[15] S. Sartyoungkul, M. Ehara, H. Sakurai, Time-dependent density functional theory investigation of excited state intramolecular proton transfer in tris (2-hydroxyphenyl) triazasumanene. *J. Phys. Chem. A*, 124 (2020) 1227-34. https://doi.org/10.1021/acs.jpca.9b10340

[16] I.K. Petrushenko, N.V. Shipitsin, K.B. Petrushenko, N-substituted sumanene and cation-π interactions towards Li cations: A theoretical study. *Physica E*, 135 (2022) 114949. https://doi.org/10.1016/j.physe.2021.114949

[17] S. Alvi, R. Ali, Synthetic approaches to bowl-shaped π-conjugated sumanene and its congeners. *Beilstein J. Org. Chem.*, 16 (2020) 2212-2259. https://doi.org/10.3762/bjoc.16.186

[18] P. Geerlings, F. De Proft, W. Langenaeker, Conceptual density functional theory. *Chem. Rev.*, 103 (2003) 1793-1874. https://doi.org/10.1021/cr990029p

[19] G.M.J. Barca, Recent developments in the general atomic and molecular electronic structure system. *J. Chem. Phys.*, 152 (2020) 154102. https://doi.org/10.1063/5.0005188

[20] D. Zheng, F. Wang, Performing molecular dynamics simulations and computing hydration free energies on the B3LYP-D3 (BJ) potential energy surface with adaptive force matching: a benchmark study with seven alcohols and one amine. *ACS Phys. Chem. Au*, 1 (2021) 14-24. https://doi.org/10.1021/acsphyschemau.1c00006

[21] M.P. Andersson, P. Uvdal, New scale factors for harmonic vibrational frequencies using the B3LYP density functional method with the triple-ζ basis set 6-311+ G (d, p). *J. Phys. Chem. A*, 109 (2005) 2937-2941. https://doi.org/10.1021/jp045733a

[22] G. Ricardo, R.R. Marcia, H. Alireza, M. Abhijit, Spectroscopy and Dipole Moment of the Molecule C13H20BeLi2SeSi Via Quantum Chemistry using Ab Initio, Hartree-Fock Method in the Base Set CC-Pvtz and 6-311G**(3df, 3pd). *Arc. Org. Inorg. Chem. Sci.*, 3 (2018) 171.

[23] R. Kareem, M. Obaid, M.H. Kebiroğlu, O.A.H. Hamad, O. Kaygili, N. Bulut, Epinephrine Compound: Unveiling Its Optical and Thermochemical Properties via Quantum Computation Methods. *Chem. Rev. Lett.*, 6 (2023) 415-427. https://doi.org/10.22034/crl.2023.421325.1253

[24] H. Loubna, E.O. Hayat, B.N.M. Mouad, A. Mouna, R.C. Mohamed, I. Walid, et al., Study of the synthesis reactivity of flavonol derivatives using quantum calculation methods. *Chem. Rev. Lett.*, 8 (2025) 388-403. https://doi.org/10.22034/crl.2025.485638.1460

[25] I. Vaziri, I. Amini, M.R.P. Heravi, R. Rzayev, A density functional theory study of adsorption dimethyl fumarate on the surface of the pristine of g-C3N4 and Fe, Ni and Cu decorated graphitic carbon nitride. *Chem. Rev. Lett.*, 8 (2025) 52-67. https://doi.org/10.22034/crl.2024.454286.1327

[26] R. Behjatmanesh-Ardakani, R. Rzayev, Hydrogen assisted SO2 dissociation on the Pt-doped graphene quantum dot surface: a non-periodic DFT study. *Chem. Rev. Lett.*, 8 (2025) 178-186. https://doi.org/10.22034/crl.2024.489135.1476

[27] A. Behnia, M.R.J. Sarvestani, A.A. Ibrahim, M.S. Mahdi, DFT Studies on the Nalidixic Acid Interactions with C8B6N6 Nanocluster. *Chem. Rev. Lett.*, 7 (2024) 993-1000. https://doi.org/10.22034/crl.2024.478064.1418

[28] R.O. Kareem, O. Hamad, H. Abdulrahman, Kebiroglu, B. Mohammed, B. Ahmed, Spectroscopic Properties and Computational Studies of Phosphosilicate-Doped Compounds Including (F, Cl, Br). *J. Chem. Lett.*, 5 (2024) 159-167. https://doi.org/10.22034/jchemlett.2024.467720.1212

[29] T.T. Uzah, I.J. Mbonu, Insight into synergistic corrosion inhibition of thiourea and ZnCl2 on mild steel: Experimental and theoretical Approaches. *J. Chem. Lett.*, 4 (2024) 211-221. https://doi.org/10.22034/jchemlett.2024.413932.1135

[30] F. Iorhuna, A.M. Ayuba, A.T. Nyijime, Comparative study of skimmianine as an adsorptive inhibitor on Al (110) and Fe (111) crystal surface, using DFT and simulation method. *J. Chem. Lett.*, 4 (2023) 148-155. https://doi.org/10.22034/jchemlett.2023.398506.1117

[31] R.L. Hsian, V.K. Hussin, O.A. Hamad, R.O. Kareem, Theoretical Study Chlorohydroquinone with substituted lithium via Quantum Computation Methods. *Chem. Res. Tech.*, 1 (2024) 73-77. https://doi.org/10.2234/chemrestec.2024.448968.1009

[32] P. Issofa, N.N. Eric, N.N. Njankwa, K.S.G. Claude, B.B.J. Ulrich, A. Emadak, Theoretical Mechanistic and Kinetic Study on the [1. 5]-H Shift in (Z)-hexa-1,3-diene. *Chem. Res. Tech.*, 1 (2024) 89-94. https://doi.org/10.22034/chemrestec.2024.449583.1012

[33] M.S. Zyane, H. Rghioui, A. Achahbar, O. Boujibar, F.T. Van, M. Zanouni, et al., A novel lithium-decorated GeC5 monolayer for promising hydrogen storage: A DFT study. *Int. J. Hydrogen Energy*, 114 (2025) 131-141. https://doi.org/10.1016/j.ijhydene.2025.03.022

[34] X. Li, G. Zhao, K. Xie, P. Wang, C. Zhang, L. Lin, Cu-decorated HfS2 and Cu-embedded HfS2 for adsorption and gas sensing of lithium-ion thermal runaway gases: A DFT study. *Surfaces and Interfaces*, 46 (2024) 104028. https://doi.org/10.1016/j.surfin.2024.104028

[35] Z. Liu, W. Zhao, M. Chai, Li-decorated bilayer borophene as a potential hydrogen storage material: a DFT study. *Int. J. Hydrogen Energy*, 51 (2024) 229-235. https://doi.org/10.1016/j.ijhydene.2023.11.093

[36] A. Seth, S.S. Gattu, K.V.S. Srinivasan, R. Sujith, Enhanced H2 storage in silicene through lithium decoration and single vacancy and Stone-Wales defects: A density functional theory investigation. *Energy Storage*, 6 (2024) e620. https://doi.org/10.1002/est2.620

[37] A. Rehman, Z. Razaaq, M. Tanveer, M.K. Masood, N. Bano, M. Shakil, Li-decorated 2D Aluminium Phosphide monolayer for hydrogen storage capacity: Insights from DFT computations. *J. Phys. Chem. Solids*, 199 (2025) 112497. https://doi.org/10.1016/j.jpcs.2024.112497

[38] S. Nikmanesh, S. Srinivasan, R. Safaiee, Ti-Decorated SiC2 as a High-Performance Anode Material for Li-ion Batteries: A DFT-D2 Approach. *Mater. Today Phys.*, 22 (2025) 101734. https://doi.org/10.1016/j.mtphys.2025.101734